



Chemical Radiation and Soret Effects on Unsteady MHD Convective Flow of Jeffrey Nanofluid Past an Inclined Semi-Infinite Vertical Permeable Moving Plate

Konduru Venkateswara Raju¹ , Ravuri Mohanaramana² , S. Sudhakar Reddy¹  and Kodi Raghunath^{*1,3} 

¹ Department of BS&H (Mathematics), S. V. College of Engineering (Autonomous), Karakambodi Road, Tirupati 517507, Andhra Pradesh, India

² Department of BS & H (Mathematics), Narasaraopeta Engineering College, Narasaraopeta 522601, Andhra Pradesh, India

³ St. Johns College of Engineering and Technology, Yemmiganur, Kurnool District, Andhra Pradesh 518360, India

*Corresponding author: kraghunath25@gmail.com

Received: March 8, 2022

Accepted: October 3, 2022

Abstract. An unsteady, MHD incompressible water-based Jeffrey nanofluid (Cu and TiO₂) flow across a stretched sheet in a transverse magnetic domain, thermic radiation, and Soret effects are examined in this article. For each physical parameter, the governing differential equalisations are converted into a set of nonlinear associated standard differential equalisations, translated utilising a perturbation approach with suitable limit essentials for the governing differential equations. The solution for the governing nonlinear boundary value concern is conveyed based on the perturbation technique throughout the complete range of material parameters. The impacts of numerous biological factors on the dimensionless velocity, temperature, concentration, and pressure silhouettes are graphically displayed and thoroughly examined. It is possible to gain favourable comparisons with formerly publicised work on several particular topic situations. Finally, numerical significances of material portions, such as the local skin-friction specification, the Nusselt numeral, and the Sherwood digit, are provided in tabular form, allowing easy comparison.

Keywords. MHD, Chemical reaction, Heat transfer, Radiation, Porous media, Soret effect

Mathematics Subject Classification (2020). 76B15, 76W05, 76S05, 76R50

1. Introduction

Many nanofluid convective heat transfer applications are already available, and the phenomenon plays an essential role in both research and engineering. They have a wide range of applications in practically every technology that uses warmth transfer liquids (either for cooling or heating), including solar power, nuclear reactors, and other similar technologies. As a result, researchers in fluid dynamics have taken a particular interest in nanofluids in current years, owing to the broad scope of applications they have in numerous sectors. It is a fact that, when compared to metals, the heat conductivity of the most regularly used fluids is low. Because of this, mixing fluids with metal particles (nano-sized) is necessary to increase the warmth transfer capabilities of the liquids. The nanofluid is a suspension of micro-sized molecules in a base liquid composed mainly of water. Choi and Eastman [6] came up with the notion of nanofluids while doing research at Argonne National Laboratory on cooling methods. The term nanofluid refers to miscellaneous liquids, including methodology extraction and environmental, biological, and medicinal nanofluids. On the thermal conductivity of nanofluids, it is essential to consider the particle fabric, particle measure, base liquid fabric, temperature, PH significance of the base liquid, particle magnitude concentration, and particle volume concentration. Many different uses for natural convection heat transfer via porous media exist, including warmth exchangers, edifice installations, geothermal energy, and oil recovery. When calculating the viscosity of a fluid, the theory of rotational flow may be quite valuable. It has been shown in several studies that supplementing the magnitude fraction of microparticles in nanofluids would direct to an expansion in the thermal conductivity of the nanofluids themselves.

Although the nanoparticles and base fluids are essential, the nanoparticles' size, shape, and volume fraction are also necessary to determine their thermal conductivity effectiveness. Initially, Choi *et al.* [7] discovered that adding a tiny number of microparticles to the base fluids would boost the thermal conductivity of the base fluids. The unstable MHD limit layer outpour over a heartwarming upright permeable surface with nanofluids under a constant transverse magnetic domain, heat radiation absorption, and a constant transverse magnetic domain was explored by Krishna *et al.* [20], and the findings were reported in Nature Communications. Sivasankaran *et al.* [31] used numerical simulation to investigate the magnetohydrodynamic cross convection outpour and warmth transmission of Cu–water nanofluids in an unbiased cavity loaded with a Darcian permeable medium and a partisan identification in a Darcian porous medium filled with a partisan label in a Darcian penetrable medium replenished with a partial slip. Many researchers have explored the limit layer investigation for cross convection via an upright wedge in an impermeable medium saturated with a power-law ilk non-Newtonian nanofluid has been explored by many researchers, including Chamkha *et al.* [4], who conducted their study in a vertical wedge. A survey conducted by Chamkha *et al.* [5] examined the consequence of invariant sideways mass outpour on non-Darcy unpretending convection of a non-Newtonian liquid along an upright cone entrenched in a replenished penetrable medium with a nanofluid. A recent study by Nandi *et al.* [23] investigated the features of 3D magneto-

convective non-linear radiative Williamson nanoliquid outpour with activation significance, numerous slips, the Hall impact and other phenomena. Das *et al.* [10] investigated the itinerant MHD convective flow associated with the warmth and mass transfer of Williamson nanoliquid over a prolonged sheet in a chemical response. Singha *et al.* [30] investigated the Soret and Dufour consequences on hydromagnetic outpour of H₂O-Based nanoliquids generated by an exponentially extending sheet soaked in a non-Darcian penetrable medium with Navier's slip edge circumstances. In their study, Seth and Mishra [27] looked into the research of the ephemeral outpour of MHD nanoliquid using a nonlinearly expanding sheet, which they found to be rather interesting. The consequences of diffusion-thermo, radiation-absorption, and hall and ion slip on MHD free convective rotating outpour of nanoliquids (Ag and TiO₂) were investigated by Krishna and Chamkha [16]. Krishna and Chamkha [17] explored the MHD squeezing outpour of water established nanoliquid via a soaked permeable medium between two similar discs regarding the Hall draft. According to Krishna and Chamkha [18], the consequence of Hall and ion slip on the unstable MHD convective rotating outpour of nanoliquids in an unsteady MHD convective rotating flow has been investigated. Using a permeable exponentially extending porous surface, Krishna [15] investigated the continuous magnetohydrodynamic convective outpour of a viscous nanoliquid caused by a porous exponentially stretching consistency, which is comparable to that of a porous exponentially trying surface. Krishna *et al.* [19] examined the consequence of radiation absorption on the MHD convective outpour of nanoliquids over a perpendicularly moving porous plate. Their findings were published in the journal Nature Communications. Krishna *et al.* [21] investigated Casson hybrid nanoliquids' unsteady radiative MHD flow over an exponentially revved upright penetrable surface.

Many industries, such as the power and chemical process industries, have potential applications for this flow type, while Prasad *et al.* [24] explored the consequences of Diffusion thermic, radioactivity absorption, and biochemical processes on the MHD unrestricted convection flow heat transport flow of a nanoliquid confined by a semi-unbounded sheet of metal, Samrat *et al.* [26] scrutinized the impact of thermic radioactivity on an Uncertain Casson Nanoliquid. Kodi *et al.* [14, 25], and Raghunath *et al.* [13] have explored the consequence of biochemical changes on the flow geometries of fluids migrating at varying speeds. The impacts of Soret on the transient composite convection outpour of viscous incompressible liquid in the existence of highly porous bordered by an abrupt endless moving scale were reviewed by Vaddemani *et al.* [33] underneath the consequence of thermic dispersion, biochemical change, and a warmth conception. The impact of frictional warmth on cross convection of a chemically responding radiative Casson nanoliquid over a predisposed permeable layer has been explored by Sulochana *et al.* [32].

The configuration of fins, steel moving mills, nuclear energy manufacturers, gas turbines, and other propulsion machines are all examples of how radiation warmth and mass transmission are used in the manufacturing industry; these techniques are also used in the creation of various propulsion devices that are used in an airliner, projectiles, satellites, and space conveyances, among other things. In the industrial sector, the impact of radiation on MHD

outpour, warmth transfer, and mass transfer are becoming more critical to understand. Numerous operations in the engineering profession occur at heightened temperatures, making the wisdom of radiation warmth transfer essential for devising the supplies used to carry out these operations. The heat-regulating components have a considerable influence on the overall quality of the finished product. It is possible to produce the desired end with the required features by correctly understanding radiative warmth transmission in a approach if the process is carried out appropriately. Several research studies have been conducted to determine the consequence of heat radiation on various outpour conditions. Previously, Cortell [8] investigated the consequences of viscous immoderation and radiation on the thermic border layer over a nonlinearly stretching sheet and the thermal boundary coating over a linearly stretching sheet in the existence of a thermic frontier layer. Ibrahim *et al.* [12] have investigated a semi-unbounded vertical permeable moving plate with a heat source and suction to determine the influence of chemical response and radiation absorption on the unsteady MHD free convection flow across it. Thermic radiation and buoyancy outcomes on warmth and mass transport across a semi-unbounded extending cover with suction and blowing have been demonstrated by Shateyi [28]. Thermic radiation and buoyancy outcomes on heat and mass transport across a semi-unbounded extending consistency can be observed using suction and blowing. Shateyi *et al.* [29] investigated the influence of thermic radiation on warmth and mass transport over an inconsistent overstated surface by measuring the temperature of the surface. Aliakbar *et al.* [3] evaluated the persuasion of heat emission on the Maxwellian fluids flow above stretching sheets in the presence of stretching sheets by measuring the temperature of the juices. Mahanthesha *et al.* [22] have investigated nonlinear emission warmth transport in the three-dimensional outpour of water established nanoliquid over a nonaligned span sheet. The consequences might be very dramatic when there is a significant shift in density in the flow regime. In some instances, such as when a species with a distinct thickness than the surrounding liquid is introduced at the fluid domain surface of a fluid domain, the Soret effect may be rather significant (see Figure 1).

The Soret effect is discussed in detail for the first time in this report. Because of the unstable magnetohydrodynamic flow passing through an abrupt penetrable comforting platter in radiation and Soret influences, the equations that regulate the outpour are recast into a set of nonaligned differential equalization, which is then decrypted using Matlab software and a perturbation approach. When a transversal magnetic domain is present, the plating is presumed to be flowing through a consistent penetrable material with invariant velocity in the directive of outpour. It moves with uniform velocity in the direction of flow. When several physical parameters are available, exact formulas for velocity, temperature, and concentration are obtained and explored using graphs in Figure 1. The consequences of varied specifications on the skin friction and the rate of heat and mass transport at the consistency are explored in tables. Comparative studies with formerly disseminated work have been conducted, and it has been revealed that the results are highly consistent with one another.

2. Mathematical Formulation

We decided to assume the outpour of a laminar, viscous, impenetrable, electrically carrying, double-diffusive, and absorbing liquid past a semi-endless upright penetrable relocation platter implanted in a constant permeable material and confined to a homogeneous transversal magnetic domain in the existence of therm radiation and a homogeneous chemical response in this channel as unsteady MHD two-dimensional flows in this channel. In this scenario, it is presumed that there is no electric potential, which indicates that there is no electrical field present at the time of assessment. Based on this assumption, the magnetic domain and the magnetic Reynolds numeral applied transversely are minimal. Consequently, the induced magnetic fields and the Hall Effect are kept to a very bare minimum. This is done by taking the y -axis upward and parallel to the flow and then taking the y^* -axis in a direction perpendicular to the flow. In this scenario, it is presumed that there is no involved voltage, which indicates that there is no electrical field present at the time of calculation. Aside from the influence of density on temperature, which is intended to be changeable, the fluid characteristics are presumed to be invariant. Therefore, the Soret consequences are not considered since the concentrations of diffusing species are so small analogised to other chemical species, and the attention of species far out from wall C^∞ is so insignificant that they are entirely neglected. Assuming that the chemical reaction happens in the flow, the linear acceleration equation is corresponded using the Boussinesq approximation. The flow theory calculates the thermophysical parameters on the linear momentum equation (see Figure 1). After making a reasonable assumption about the semi-endless plane consistency, the outpour variables may be reduced to simple processes of the variables y^* and time t^* .

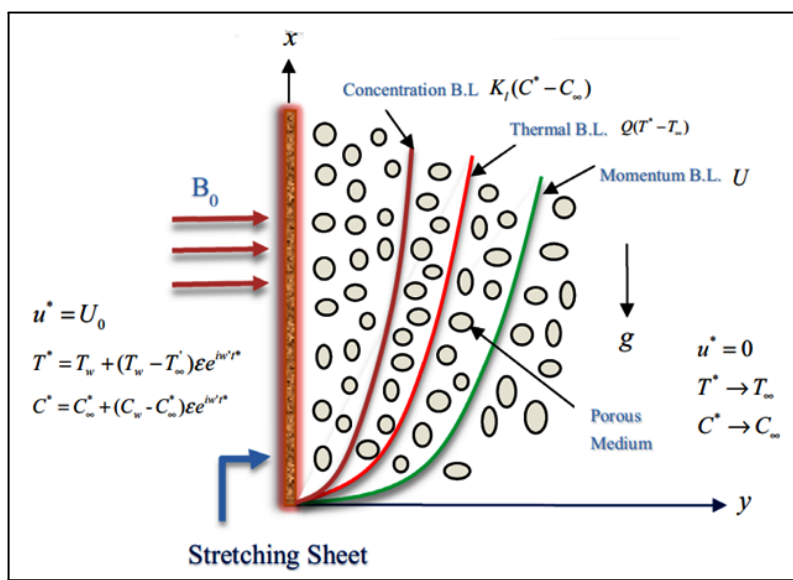


Figure 1

Figure 1 diagram that shows how the issue is physically structured

$$\frac{\partial v^*}{\partial y^*} = 0 \rightarrow v^* = -v_0 \quad (v_0 > 0), \tag{2.1}$$

$$\begin{aligned} \rho_{nf} \left(\frac{\partial u^*}{\partial t^*} + v^* \frac{\partial u^*}{\partial y^*} \right) = & -\frac{1}{\rho_{nf}} \left(\frac{1}{1+\lambda} \right) \frac{\partial p^*}{\partial x^*} + \mu_{nf} \frac{\partial^2 u^*}{\partial y^{*2}} + (\rho\beta_T)_{nf} g(T^* - T_\infty^*) \cos \alpha \\ & + (\rho\beta_c)_{nf} g(C^* - C_\infty^*) \cos \alpha - \frac{\sigma B_0^2}{\rho_{nf}} \sin^2 \gamma u^* - \frac{\mu_{nf} u^*}{k^*}, \end{aligned} \tag{2.2}$$

$$\left(\frac{\partial T^*}{\partial t^*} + v^* \frac{\partial T^*}{\partial y^*} \right) = \alpha_{nf} \frac{K}{(\rho C_p)_{nf}} \frac{\partial^2 T^*}{\partial y^{*2}} - \frac{1}{(\rho C_p)_{nf}} \frac{\partial q_r^*}{\partial y^*} + \frac{Q^*}{(\rho C_p)_{nf}} (T^* - T_\infty^*), \tag{2.3}$$

$$\frac{\partial C^*}{\partial t^*} + v^* \frac{\partial C^*}{\partial y^*} = D \frac{\partial^2 C^*}{\partial y^{*2}} - K^* (C^* - C_\infty^*) + D_1 \frac{\partial^2 T^*}{\partial y^{*2}}, \tag{2.4}$$

where u^* and v^* are velocity segments in x^* and y^* directives respectively, on the additional pointer, β_f and β_C are the coefficients of thermal elaboration of the liquid and the substantial, ρ_f and ρ_C are the thicknesses of the liquid and the substantial scraps, respectively, while ρ_{nf} is the consistency of the nanoliquid, α_{nf} is the thermic diffusivity of the nanoliquid, and $(\rho C_p)_{nf}$ is the heat capacitance of the liquid, which are characterized as (Abbasi *et al.* [1,2]).

$$\left. \begin{aligned} \rho_{nf} &= (1-\phi)\rho_f + \phi\rho_s, \\ (\rho C_p)_{nf} &= (1-\phi)(\rho C_p)_f + \phi(\rho C_p)_s, \\ (\rho\beta)_{nf} &= (1-\phi)(\rho\beta)_f + \phi(\rho\beta)_s \end{aligned} \right\} \tag{2.5}$$

$$K_{nf} = K_f \left(\frac{K_s + 2K_f - 2\phi(K_f - K_s)}{K_s + 2K_f + 2\phi(K_f - K_s)} \right), \quad \mu_{nf} = \left(\frac{\mu_f}{(1-\phi)^{2.5}} \right), \tag{2.6}$$

$$\alpha_{nf} = \left(\frac{K_{nf}}{(\rho C_p)_{nf}} \right), \tag{2.7}$$

$$v^* = -v_0. \tag{2.8}$$

Let us consider the following theoretical formulation for an optic thin limit grey gas that is on its way to equilibrate: In their formalized version of this notion, Cramer and Pai [9] presented an example. Grief *et al.* [11] as followed

$$\frac{\partial q_r^*}{\partial y^*} = 4(T^* - T_w^*)I. \tag{2.9}$$

Under the previously stated constraints, the following equations give the boundary conditions for velocity, temperature, and concentration variations:

$$\left. \begin{aligned} U^* &= u_p^*, \quad T^* = T_u^* + \varepsilon(T_w^* - T_\infty^* e^{n^* t^*}), \quad C^* = C_w^* + \varepsilon(C_w^* - C_\infty^*) e^{n^* t^*} \quad \text{at } y^* = 0, \\ u^* &\rightarrow u_\infty^* = U_0(1 + \varepsilon e^{n^* t^*}), \quad T^* \rightarrow T_\infty^* \quad C^* \rightarrow C_\infty^* \quad \text{at } y^* \rightarrow \infty. \end{aligned} \right\} \tag{2.10}$$

Equation (2.2) yields the result outside of the boundary layer.

$$-\frac{1}{\rho_{nf}} \frac{\partial p^*}{\partial x^*} = \frac{\partial U_\infty}{\partial t^*} + \frac{v}{k^*} U_\infty^* + \frac{\sigma B_0^2}{\rho_{nf}} U_\infty^*. \tag{2.11}$$

Include the non-dimensional characteristics and attributes specified below:

$$\left. \begin{aligned} u &= \frac{u^*}{U_0}, \quad v = \frac{v^*}{v_0}, \quad y = \frac{v_0 y^*}{v_f}, \quad U_\infty = \frac{U_\infty^*}{U_0}, \quad U_p = \frac{U_p^*}{U_0}, \quad t = \frac{t^* v_0^2}{v_f}, \quad \theta = \frac{T^* - T_\infty^*}{T_w^* - T_\infty^*}, \\ \phi &= \frac{C^* - C_\infty^*}{C_w^* - C_\infty^*}, \quad n = \frac{n^* \vartheta_f}{v_0^2}, \quad k = \frac{k^* v_0^2}{v_f^2}, \quad Pr = \frac{\mu_f C_{pf}}{K_f}, \quad Sc = \frac{v_f}{D_m}, \quad M = \frac{\sigma B_0^2 v_f}{\rho_f v_0^2}, \\ Q &= \frac{Q^* v_f}{(\rho C_p)_f v_0^2}, \quad K = \frac{v_f K^*}{v_0^2}, \quad R = \frac{4I_1 v_f}{(\rho C_p)_f v_0^2}, \quad S_r = \frac{D_1, K(T_w^* - T_\infty^*)}{v_f (C_w^* - C_\infty^*)}, \\ Gr &= \frac{v_f g(\rho \beta_T)_f (T_w^* - T_\infty^*)}{U_0 v_0^2}, \quad Gm = \frac{v_f g(\rho \beta_c^*)_f (C_w^* - C_\infty^*)}{U_0 v_0^2}, \quad S = \frac{v_0}{U_0}. \end{aligned} \right\} \quad (2.12)$$

In the non-dimensional version, the equations (2.2) to (2.4) are as follows:

$$\begin{aligned} \left((1 - \phi) + \phi \left(\frac{\rho_s}{\rho_f} \right) \right) \left(\frac{\partial u}{\partial t} - S \frac{\partial u}{\partial y} \right) &= \frac{dU_\infty}{dt} + \left(\frac{1}{(1 - \phi)^{2.5}} \right) \left(\frac{1}{1 + \lambda} \right) \frac{\partial^2 u}{\partial y^2} \\ &+ \left((1 - \phi) + \phi \left(\frac{(\rho \beta)_s}{(\rho \beta)_f} \right) \right) (Gr \theta + Gm \phi) \cos \alpha \\ &+ (M \sin^2 \gamma + 1/k)(U_\infty - u), \end{aligned} \quad (2.13)$$

$$\left((1 - \phi) + \phi \left(\frac{(\rho C_p)_s}{(\rho C_p)_f} \right) \right) \left(\frac{\partial \theta}{\partial t} - S \frac{\partial \theta}{\partial y} \right) = \frac{1}{Pr} \left(\left(\frac{(1 + 2\phi) + (2 - 2\phi) \left(\frac{K_f}{K_s} \right)}{(1 - 2\phi) + (2 + 2\phi) \left(\frac{K_f}{K_s} \right)} \right) \frac{\partial^2 \theta}{\partial y^2} - (R + Q)\theta \right), \quad (2.14)$$

$$\frac{\partial \phi}{\partial t} - S \frac{\partial \phi}{\partial y} = \frac{1}{Sc} \frac{\partial^2 \phi}{\partial y^2} + Sr \frac{\partial^2 \phi}{\partial y^2} - K \phi. \quad (2.15)$$

The limit requirements for this scenario are as follows:

$$\left. \begin{aligned} u &= U_p, \quad \theta = 1 + \varepsilon e^{nt}, \quad \phi = 1 + \varepsilon e^{nt}, \quad \text{at } y = 0, \\ u &= U_\infty = 1 + \varepsilon e^{nt}, \quad \theta \rightarrow 0, \quad \phi \rightarrow 0, \quad \text{as } y \rightarrow \infty. \end{aligned} \right\} \quad (2.16)$$

3. Method of Solution

The partial differential equations (2.10)-(2.12) are a collection of equalisations that cannot be translated into a closed-form. But by lowering them to many standard differential equations and translating them utilising the perturbation strategy depicted below. Now, in stints of harmonic and non-harmonic positions, characterise the velocity, temperature, and concentration distributions as

$$\left. \begin{aligned} U(y, t) &= u_0(y) + \varepsilon u_1(y) e^{nt} + O(\varepsilon^2), \\ T(y, t) &= \theta_0(y) + \varepsilon \theta_1(y) e^{nt} + O(\varepsilon^2), \\ C(y, t) &= \phi_0(y) + \varepsilon \phi_1(y) e^{nt} + O(\varepsilon^2). \end{aligned} \right\} \quad (3.1)$$

3.1 Zero Order Terms

$$D \lambda_1 u_0'' + S u_0' - \xi u_0 = -B Gr \cos \alpha \theta_0 - Gm \cos \alpha \phi_0 - (M \sin^2 \gamma + 1/k), \quad (3.2)$$

$$E \theta_0'' + C Pr \theta_0' - (F + Q) Pr \theta_0 = 0, \quad (3.3)$$

$$\varphi_0'' + Sc \varphi_0' - Sc K \varphi_0 = -Sc Sr \theta_0'' \quad (3.4)$$

3.2 First Order Terms

$$D \lambda_1 u_1'' + S u_1' - ((M + 1/k) + n) u_1 = -B Gr \cos \alpha \theta_1 - Gm \cos \alpha \phi_1 - S u_0' - (M \sin^2 \gamma + 1/k) + n, \quad (3.5)$$

$$E \theta_1'' + C Pr \theta_1' - (n + (M \sin^2 \gamma + 1/k)) Pr \theta_1 = -Pr S \theta_0', \quad (3.6)$$

$$\varphi_1'' + Sc \varphi_1' - Sc(K + n) \varphi_1 = -S Sc \varphi_0' - Sc Sr \theta_1'', \quad (3.7)$$

The boundary conditions that relate to this are as follows:

$$\left. \begin{aligned} u_0 = U_p, \quad u_1 = 0, \quad \theta_0 = 1, \quad \theta_1 = 1, \quad C_0 = 1, \quad C_1 = 1, \quad \text{at } y = 0, \\ u_0 = 1, \quad u_1 = 1, \quad \theta_0 \rightarrow 0, \quad \theta_1 \rightarrow 0, \quad C_0 \rightarrow 0, \quad C_1 \rightarrow 0 \quad \text{as } y \rightarrow \infty. \end{aligned} \right\} \quad (3.8)$$

The following answers are derived by solving equations (3.2)-(3.7) under the boundary conditions (3.8), which are as follows:

$$u_0 = 1 + b_9 \exp(-m_5 y) + b_{10} \exp(-m_3 y) + b_{11} \exp(-m_5 y), \quad (3.9)$$

$$u_1 = 1 + b_9 \exp(-m_5 y) + b_{10} \exp(-m_3 y) + b_{11} \exp(-m_5 y), \quad (3.10)$$

$$\theta_0 = \exp(-m_1 y), \quad (3.11)$$

$$\theta_1 = b_1 \exp(-m_1 y) + b_2 \exp(-m_2 y), \quad (3.12)$$

$$\varphi_0 = b_3 \exp(-m_1 y) + b_4 \exp(-m_3 y), \quad (3.13)$$

$$\varphi_1 = b_5 \exp(-m_1 y) + b_6 \exp(-m_2 y) + b_7 \exp(-m_3 y) + b_8 \exp(-m_4 y). \quad (3.14)$$

Compute the velocity, temperature, and concentration dispersal in the frontier layer by superseding equations (3.6)-(3.11) into (2.14), as exhibited downward:

$$u = (1 + b_9 \exp(-m_1 y) + b_{10} \exp(-m_3 y) + b_{11} \exp(-m_5 y)) + \varepsilon e^{nt} (1 + b_{12} \exp(-m_1 y) + b_{13} \exp(-m_2 y) + b_{14} \exp(-m_3 y) + b_{15} \exp(-m_4 y) + b_{16} \exp(-m_5 y) + b_{17} \exp(-m_6 y)), \quad (3.15)$$

$$\theta = \exp(-m_1 y) + \varepsilon e^{nt} (b_1 \exp(-m_1 y) + b_2 \exp(-m_2 y)), \quad (3.16)$$

$$\phi = b_3 \exp(-m_1 y) + b_4 \exp(-m_3 y) + \varepsilon e^{nt} (b_5 \exp(-m_2 y) + b_6 \exp(-m_2 y) + b_7 \exp(-m_3 y) + b_8 \exp(-m_4 y)). \quad (3.17)$$

3.3 Skin Friction

The skin friction, which is an extremely significant material specification near the frontier, is represented in non-dimensional form and may be calculated as follows:

$$\tau = \left(\frac{\partial u}{\partial y} \right)_{y=0},$$

$$\tau = -(m_1 b_9 + m_3 b_{10} + m_5 b_{11}) - \varepsilon e^{nt} (m_1 b_{12} + m_2 b_{13} + m_3 b_{14} + m_4 b_{15} + m_5 b_{16} + m_6 b_{17}). \quad (3.18)$$

3.4 Nusselt Number

The rate of heat transfer stated in the form of the Nusselt number, is expressed by the formula:

$$Nu = - \left(\frac{\partial \theta}{\partial y} \right)_{y=0} = -m_1 - \varepsilon e^{nt} (m_1 b_1 + m_2 b_2). \quad (3.19)$$

3.5 Sherwood Number

The rate of mass transfer, expressed in terms of the Sherwood number, may also be calculated:

$$Sh = - \left(\frac{\partial C}{\partial y} \right)_{y=0},$$

$$Sh = m_1 b_3 + m_3 b_4 + \varepsilon e^{nt} (m_1 b_5 + m_2 b_6 + m_4 b_7 + m_5 b_8). \tag{3.20}$$

4. Results and Discussion

By allocating specific significance to the parameters penetrating the concern, we could acquire biological wisdom into the problem by assuming numerical computations for non-dimensional velocity, temperature and species concentration, skin-friction, and Nusselt number to develop material insight into the problem for two distinct varieties of water-based nanoliquids. We confirmed dual resolutions for nanoliquids made of TiO₂-water and CuO-water.

Figures 2 through 15 have been included for this reason. Table 1 depicts the thermophysical parameters of water and the Nano-elemental composition (Cu and TiO₂). The skin friction coefficient and local Nusselt number were compared with those reported by Samrat *et al.* [26] for various values to evaluate the validity and precision of the current findings. The results of this comparison are shown in Table 2, and it was discovered that they were in perfect accord. Therefore, we are convinced that the current findings are more accurate than those obtained before.

Figure 2 and 3 depicts the behaviour of the angle of inclination and aligned magnetic field on a velocity profile, which can be seen in Figure 2 and Figure 3, respectively. It can be seen that raising the value of inclination and aligned magnetic field specifications, causes the velocity profile to drop. Because the influence of the magnetic field on fluid particles increases with increasing angle of inclination, the Lorentz force is amplified as the angle of inclination rises. As a result, the velocity profile becomes narrower.

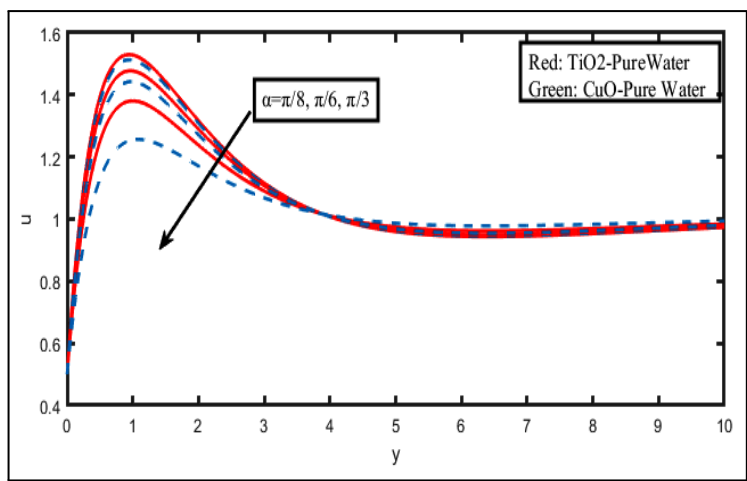


Figure 2. Velocity profile for inclined parameter α

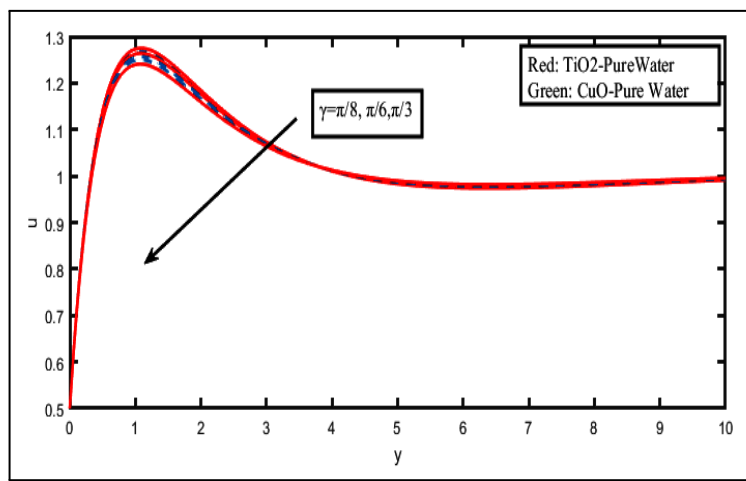


Figure 3. Velocity profile for Aligned magnetic field parameter

Table 1. Thermo-physical properties (see [24, 26])

Physical properties	Water	Copper (Cu)	Titanium Oxide (TiO ₂)
C_p (J/Kg K)	4179	385	686.2
ρ (Kg/m ³)	997.1	8933	4250
k (w/m K)	0.613	400	8.9538
$\beta * 10^{-5}$ (1/K)	21	1.67	0.9

According to Figure 4, greater values of the Jeffrey fluid parameter have a propensity to slow down the fluid flow in the case of Cu-water and TiO₂-water nanofluids, respectively. According to the predictions, increasing will be used to lower the yield stress, which will raise the value of plastic dynamic viscosity, which will cause resistance to the flow of liquids and other fluids. It should be mentioned that owing to the flexibility of Jeffrey fluid, the non-Newtonian behaviours of the fluid vanish, and the fluid behaves exclusively as a Newtonian fluid when it is applied.

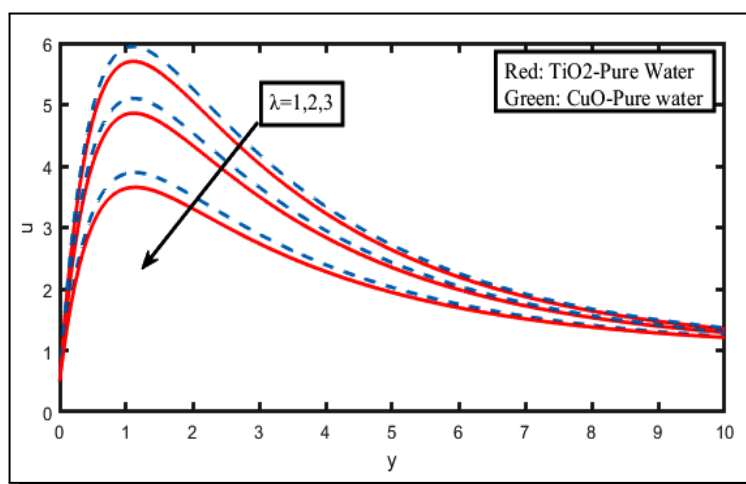


Figure 4. Velocity profile for Jeffrey fluid parameter λ

Figure 5 depicts the influence of a magnetic field parameter on the velocity of Cu-water and TiO₂-water nanofluids, which are both dissolved in water. In response to an increase in the magnetic parameter, the velocity profiles of both nanofluids drop. A retarding Lorentz force is produced by introducing a transverse magnetic field in an electrically conducting fluid, which explains why this occurs. It is believed that this force is responsible for slowing down fluid motion in the boundary layer and reducing velocity. A similar effect has been seen by Prasad *et al.* [24].

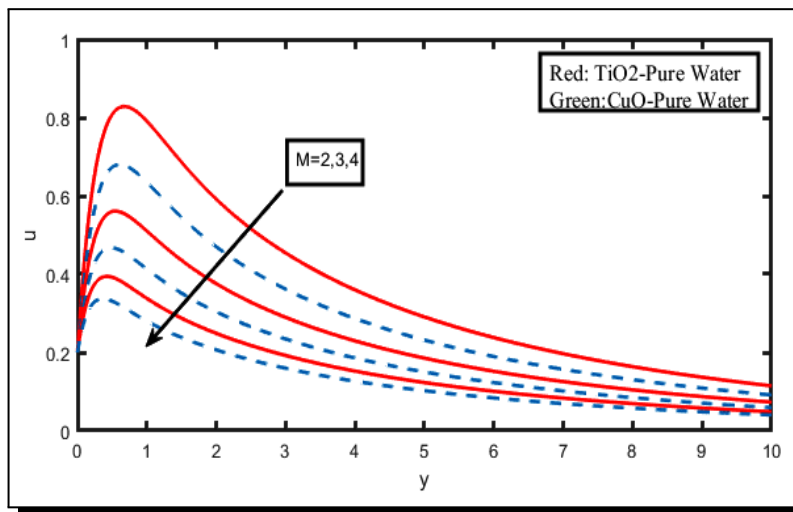


Figure 5. Velocity profile for Magnetic field M

As can be seen in Figures 6 and 7, increasing the Grashof numeral (Gr) and modified Grashof numeral (Gm) increases the velocity in the case of Cu-water and TiO₂-water nanofluids. This indicates that the current investigation is a buoyancy obliging outpour with thermic buoyancy and mass buoyancy invariant with Sulochana *et al.* [32].

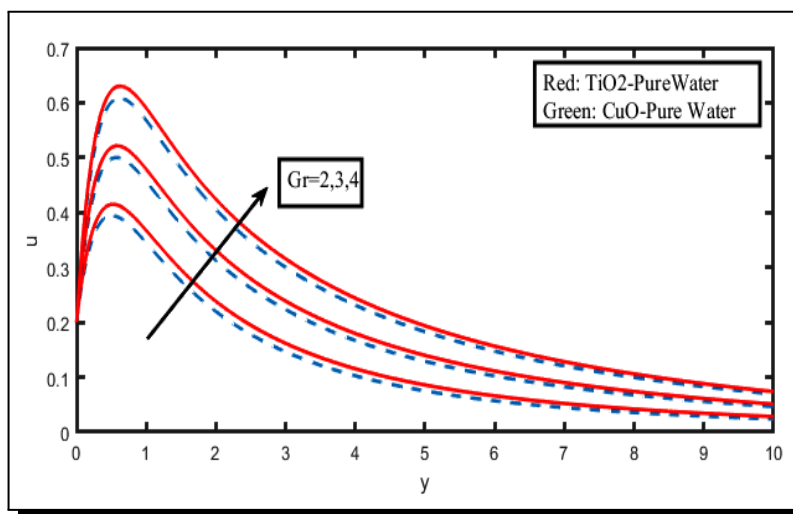


Figure 6. Velocity profile for thermal Grashof number Gr

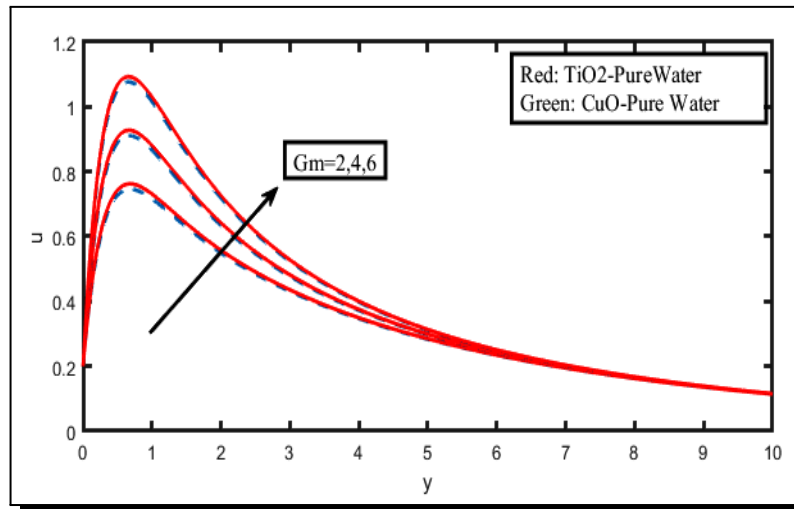


Figure 7. Velocity profile for mass Grashof number Gm

On the other hand, Figures 8 and 10 show the consequence of a radiation specification on the velocity and temperature silhouettes, respectively. It can be glimpsed from these figures that, when the radiation parameter was increased, we saw an expansion in the velocity and temperature silhouettes of the flow but a decline in the flow. With an increase in the radiation parameter, heat energy is released into the flow, which contributes to the rise in the temperature and velocity profiles of the flow.

Figures 9 and 13 are representations of the influence of the soret parameter (Sr) on the velocity and concentration fields of the flow in the relevant figures. It is undeniable that increasing the amount of Sr in the atmosphere enhances the velocity and concentration of the frontier coating. Physically, a mass flow is formed from the differential in concentration species when a heat gradient is present; this happens in the Soret effect. According to Sulochana *et al.* [32], they also noticed a similar outcome.

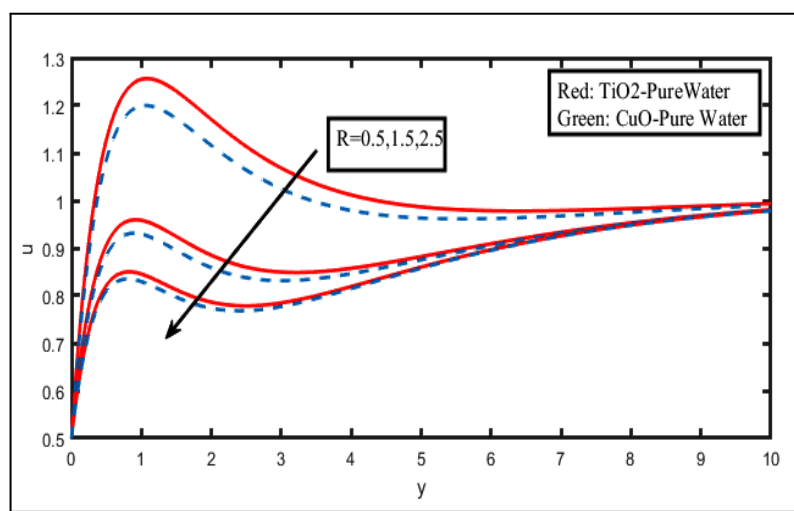


Figure 8. Velocity profile for Radiation parameter (R)

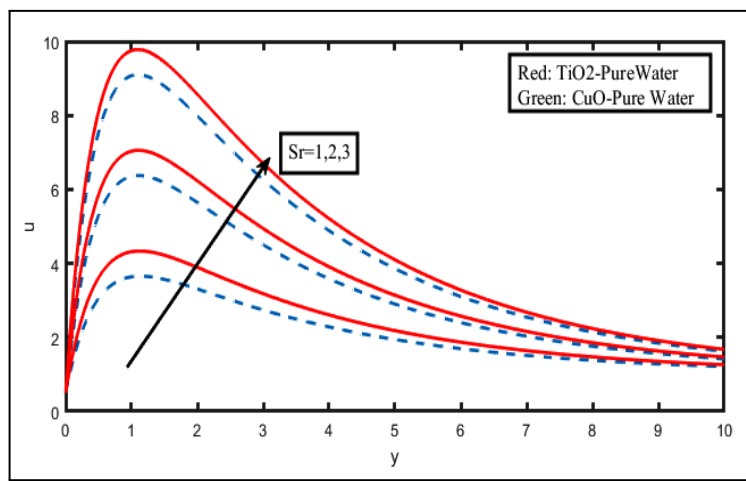


Figure 9. Velocity profile for Soret parameter (Sr)

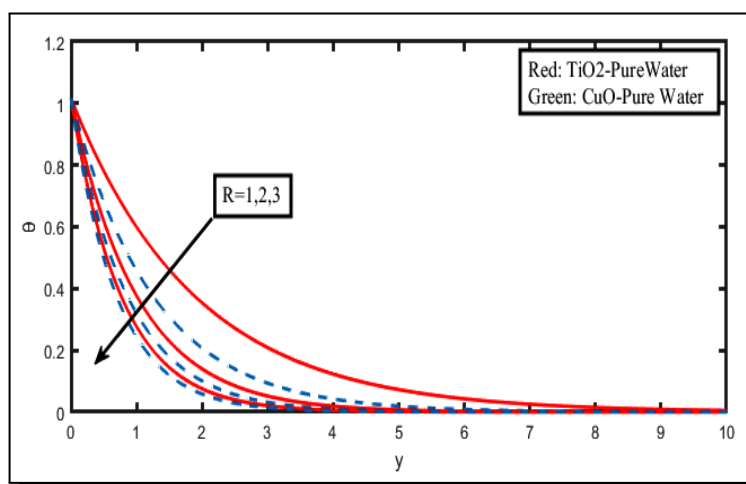


Figure 10. Temperature profile for radiation parameter (R)

The results have been as predicted regarding the consequence of the Prandtl numeral on the temperature silhouette. Increasing values of Prandtl numeral, the consistency of the thermic and solute edge layers decreases, as seen in Figure 11. This conclusion is congruent with Mahantesh *et al.* [22], who achieved similar results.

An illustration of the influence of a heat origin specification on the temperature silhouette is shown in Figure 12. We noticed effects comparable to those we had seen for the radiation specification. It complies with the material reality that increasing the heat source specification diminishes the thickness of the thermic barrier layer while simultaneously increasing the heat transfer rate.

The fluctuation in the concentration limit coating of the outpour domain for H_2 , H_2O vapour, and NH_3 is depicted in Figure 14 for the three gases. The concentration distribution in the presence of a flow field is shown in this image. When the curves in the above figure are compared, it can be seen that the increasing Schmidt numeral causes the concentration limit coating consistency of the flow domain to decrease at all places in the flow field.

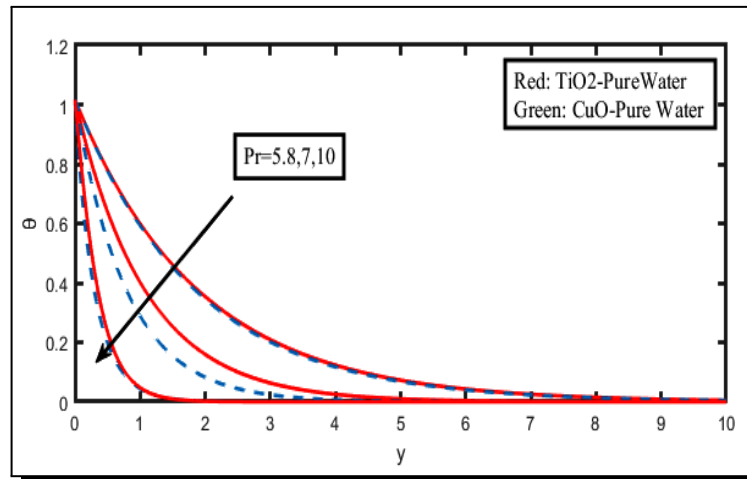


Figure 11. Temperature profile for Prandtl number parameter (Pr)

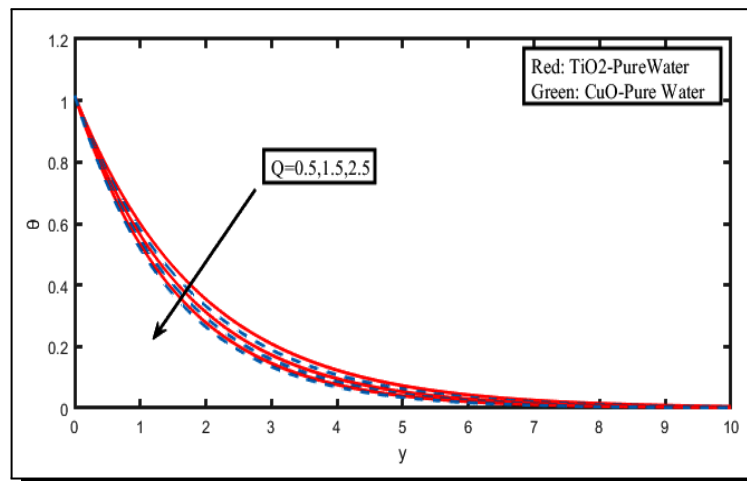


Figure 12. Temperature profile for Heat source parameter (Q)

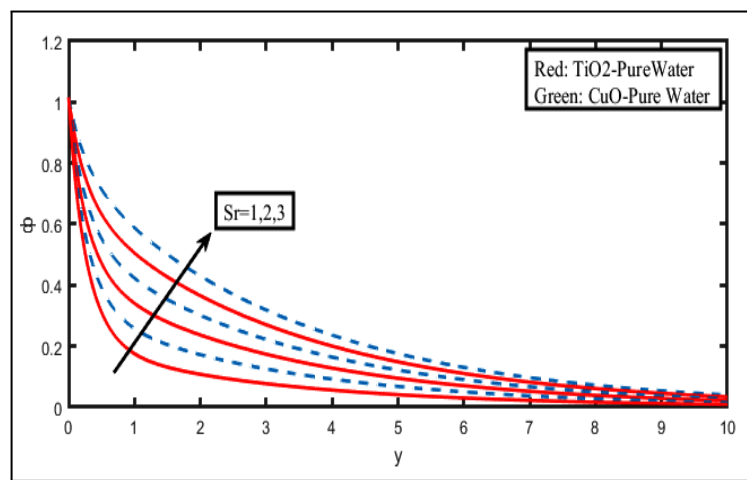


Figure 13. Concentration profile for Soret parameter (Sr)

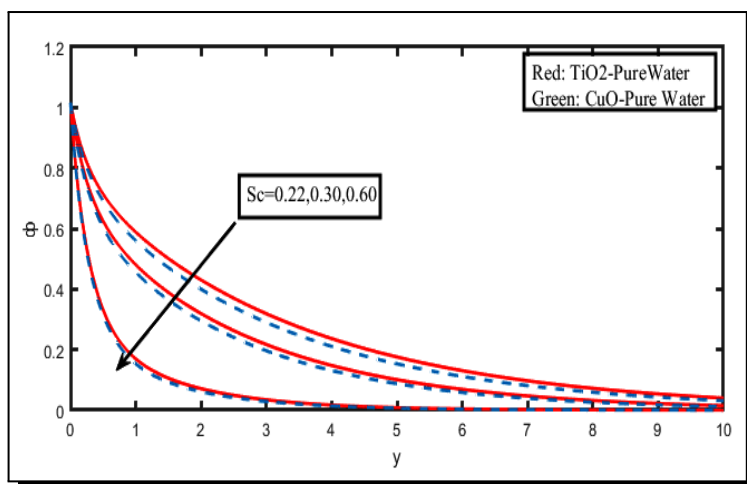


Figure 14. Concentration profile for Schmidt number parameter (Sc)

Figure 15 illustrates the consequence of a chemical response specification on concentration silhouettes as a function of time. It is clear from the statistics that a rise in the chemical response specification causes a decrease in the concentration silhouette of the fluid flow. According to the typical physical behaviour of chemical reaction parameters, this is the case, which decreases as the chemical reaction progresses.

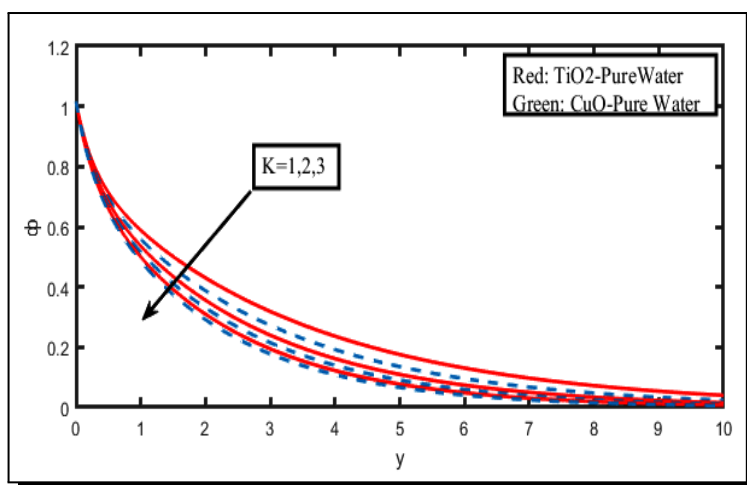


Figure 15. Concentration profile for chemical reaction parameter (Kr)

Table 2. The impact of a multiple variables on the skin friction for $Sc = 0.60$, $Pr = 6.2$, $Gr = 5$, $k = 0.5$, $Kr = 0.1$, $M = 1$, $Q = 2$, $E = 0.01$, $S = 0.5$, $R = 0.1$, $Gm = 3$, $t = 0.5$, $n = 1$, $Up = 0.5$, $Sr = 1.5$

Gr	M	S	Sr	R	Kr	Gm	λ	Skin friction for copper water fluid (Samrat et al. [26])	Skin friction for copper water fluid — Present values	Skin friction for titanium oxide water fluid — Present values
5	1	0.5	1.5	1	0.5	3	0.5	1.6383	0.1175	0.3012
5	2	0.5	1.5	1	0.5	3	0.5	1.6120	1.9225	1.5165
5	3	0.5	1.5	1	0.5	3	0.5	1.5850	3.9568	3.3045

Table Contd.

<i>Gr</i>	<i>M</i>	<i>S</i>	<i>Sr</i>	<i>R</i>	<i>Kr</i>	<i>Gm</i>	λ	Skin friction for copper water fluid (Samrat <i>et al.</i> [26])	Skin friction for copper water fluid — Present values	Skin friction for titanium oxide water fluid — Present values
5	1	0.5	1.5	1	0.5	3	0.5	1.7287	4.2675	4.2387
5	1	1.0	1.5	1	0.5	3	0.5	1.5289	1.9475	1.5197
5	1	1.5	1.5	1	0.5	3	0.5	1.3482	0.4625	0.0446
5	1	0.5	1.5	2	0.5	3	0.5	1.3340	1.9212	1.5151
5	1	0.5	1.5	3	0.5	3	0.5	1.4107	3.0112	2.6845
5	1	0.5	1.5	1	0.5	3	1	1.4781	3.5752	3.3652
5	1	0.5	1.5	1	1.0	3	2	1.5289	0.7550	0.4525
5	1	0.5	1.5	1	1.5	3	3	1.6054	5.4653	4.6878
5	1	0.5	1.5	1	0.5	2	0.5	1.6818	10.2652	8.9598
5	1	0.5	1.5	1	0.5	4	0.5	1.5289	1.4775	1.1885
5	1	0.5	15	1	0.5	6	0.5	1.2211	1.5852	1.2446
2	1	0.5	1.5	1	0.5	3	0.5	1.0404	1.7152	1.3152
4	1	0.5	1.5	1	0.5	3	0.5	0.4917	0.0361	0.2445
6	1	0.5	1.5	1	0.5	3	0.5	0.8675	2.0575	2.1352
5	1	0.5	0.5	1	0.5	3	0.5	1.1364	2.2295	2.2678
5	1	0.5	1.5	1	0.5	3	0.5	1.5289	0.9856	0.9882
5	1	0.5	2.5	1	0.5	3	0.5	1.4927	1.9352	1.4124

Table 3. the impact of a multiple variables on the Nusselt numeral for $Pr = 6.2, Q = 2, R = 1, t = 0.5$

<i>R</i>	<i>Pr</i>	<i>Q</i>	Nusselt number for copper water fluid present values	Nusselt number for titanium oxide water fluid present values
1	6.2	2	0.4565	0.5525
2	6.2	2	0.8995	0.6145
3	6.2	2	2.2395	1.7825
1	6.2	3	0.9412	1.4645
1	6.2	4	1.4956	1.9454
1	6.2	5	2.4132	2.3751

Table 4. the impact of a multiple variables on the Sherwood numeral for $Sc = 0.60, K = 0.1, Q = 2, E = 0.01, R = 1, t = 0.5, n = 1, Sr = 1.5$

<i>Q</i>	<i>Kr</i>	<i>Sr</i>	<i>Sh</i>
1	1	1	-0.3995
2			-0.5409
3			-0.7564
1	0.1	1	-0.0864
	0.2		-0.1255
	0.3		-0.8443
1	1	1	-1.1686
		1.5	-1.0340
		2	-0.8995

5. Conclusion

The investigation of two different nanofluids, namely, TiO₂-water and CuO-water, was undertaken to make the analysis more appealing. The following are the findings and conclusions:

Raising the values of the Hartmann number, angle of inclination, Jeffrey parameter, radiation and Soret parameters reduces the resulting velocity whilst increasing the importance of the thermal and mass Grashof numbers raises it. The temperature profile becomes flattered when the Prandtl number, the heat source parameter, and the radiation parameters are increased. In the case of both nanofluids, the concentration profile is reduced by the chemical reaction parameter and the Schmidt number, while the Soret effect boosts it due to the Soret effect.

Competing Interests

The authors declare that they have no competing interests.

Authors' Contributions

All the authors contributed significantly in writing this article. The authors read and approved the final manuscript.

References

- [1] F. M. Abbasi, T. Hayat and A. Alsaedi, Peristaltic transport of magneto-nanoparticles submerged in water: Model for drug delivery system, *Physica E: Low-dimensional Systems and Nanostructures* **68** (2015), 123 – 132, DOI: 10.1016/j.physe.2014.12.026.
- [2] F. M. Abbasi, T. Hayat and F. Alsaadi, Hydromagnetic peristaltic transport of water-based nanofluids with slip effects through an asymmetric channel, *International Journal of Modern Physics B* **29**(21) (2015), 1550151, DOI: 10.1142/S0217979215501519.
- [3] V. Aliakbar, A. Alizadeh-Pahlavan and K. Sadeghy, The influence of thermal radiation on MHD flow of Maxwellian fluids above stretching sheets, *Communications in Nonlinear Science and Numerical Simulation* **14**(3) (2009), 779 – 794, DOI: 10.1016/j.cnsns.2007.12.003.
- [4] A. J. Chamkha, M. Rashad and R. S. R. Gorla, Non-similar solutions for mixed convection along a wedge embedded in a porous medium saturated by a non-Newtonian nanofluid: Natural convection dominated regime, *International Journal of Numerical Methods for Heat & Fluid Flow* **24**(5) (2014), 1471 – 1786, DOI: 10.1108/HFF-07-2012-0169.
- [5] A. Chamkha, S. Abbasbandy and A. M. Rashad, Non-Darcy natural convection flow for non-Newtonian nanofluid over cone saturated in porous medium with uniform heat and volume fraction fluxes, *International Journal of Numerical Methods for Heat & Fluid Flow* **25**(2) (2015), 422 – 437, DOI: 10.1108/HFF-02-2014-0027.
- [6] S. U. S. Choi and J.A. Eastman, Enhancing thermal conductivity of fluids with nanoparticles, in: Proceedings of the Conference “1995 International Mechanical Engineering Congress and Exhibition”, San Francisco, CA (United States), 12-17 November 1995, 99 – 105, URL: <https://www.osti.gov/servlets/purl/196525>.

- [7] S. U. S. Choi, Z. G. Zhang, W. Yu, F. E. Lockwood and E. A. Grulke, Anomalous thermal conductivity enhancement in nanotube suspensions, *Applied Physics Letters* **79** (2001), 2252, DOI: 10.1063/1.1408272.
- [8] R. Cortell, Effects of viscous dissipation and radiation on the thermal boundary layer over a nonlinearly stretching sheet, *Physics Letters A* **372**(5) (2008), 631 – 636, DOI: 10.1016/j.physleta.2007.08.005.
- [9] K. P. Cramer and S.I. Pai, *Magneto Fluid Dynamics for Engineers and Applied Physics*, McGraw-Hill Book Co., New York (1973).
- [10] M. Das, B. Kumbhakar and J. Singh, Analysis of unsteady MHD Williamson nanofluid flow past a stretching sheet with nonlinear mixed convection, thermal radiation and velocity slips, *Journal of Computational Analysis and Applications* **30**(1) (2022), 176 – 195, URL:<http://www.eudoxuspress.com/images/JOCAAA-VOL-30---2022-ISSUE-1.pdf#page=176>.
- [11] R. Greif, I. S. Habib and J. C. Lin, Laminar convection of a radiating gas in a vertical channel, *Journal of Fluid Mechanics* **46**(3) (1971), 513 – 520, DOI: 10.1017/S0022112071000673.
- [12] F. S. Ibrahim, A. M. Elaiw and A. A. Bakr, Effect of the chemical reaction and radiation absorption on the unsteady MHD free convection flow past a semi infinite vertical permeable moving plate with heat source and suction, *Communications in Nonlinear Science and Numerical Simulation* **13**(6) (2008), 1056 – 1066, DOI: 10.1016/j.cnsns.2006.09.007.
- [13] R. Kodi and O. Mopuri, Unsteady MHD oscillatory Casson fluid flow past an inclined vertical porous plate in the presence of chemical reaction with heat absorption and Soret effects, *Heat Transfer* **51**(1) (2022), 733 – 752, DOI: 10.1002/htj.22327.
- [14] R. Kodi, O. Mopuri, S. Sree and V. Konduru, Investigation of MHD Casson fluid flow past a vertical porous plate under the influence of thermal diffusion and chemical reaction, *Heat Transfer* **51**(1) (2022), 377 – 394, DOI: 10.1002/htj.22311.
- [15] M. V. Krishna, Heat transport on steady MHD flow of copper and alumina nanofluids past a stretching porous surface, *Heat Transfer* **49**(3) (2020), 1374 – 1385, DOI: 10.1002/htj.21667.
- [16] M. V. Krishna and A. J. Chamkha, Hall and ion slip effects on MHD rotating boundary layer flow of nanofluid past an infinite vertical plate embedded in a porous medium, *Results in Physics* **15** (2019), 102652, DOI: 10.1016/j.rinp.2019.102652.
- [17] M. V. Krishna and A. J. Chamkha, Hall effects on MHD squeezing flow of a water-based nanofluid between two parallel disks, *Journal of Porous Media* **22**(2) (2019), 209 – 223, DOI: 10.1615/JPorMedia.2018028721.
- [18] M. V. Krishna and A. J. Chamkha, HHall and ion slip effects on unsteady MHD convective rotating flow of nanofluids – Application in biomedical engineering, *Journal of the Egyptian Mathematical Society* **28**(1) (2020), 1 – 14, DOI: 10.1186/s42787-019-0065-2.
- [19] M. V. Krishna, N. A. Ahamad and A. J. Chamkha, Radiation absorption on MHD convective flow of nanofluids through vertically travelling absorbent plate, *Ain Shams Engineering Journal* **12**(3) (2021), 3043 – 3056, DOI: 10.1016/j.asej.2020.10.028.
- [20] M. V. Krishna, N. A. Ahammad and A. J. Chamkha, Radiative MHD flow of Casson hybrid nanofluid over an infinite exponentially accelerated vertical porous surface, *Case Studies in Thermal Engineering* **27** (2021), 101229, DOI: 10.1016/j.csite.2021.101229.
- [21] M. V. Krishna, N. A. Ahammad and A. J. Chamkha, Radiative MHD flow of Casson hybrid nanofluid over an infinite exponentially accelerated vertical porous surface, *Case Studies in Thermal Engineering* **27** (2021), 101229, DOI: 10.1016/j.csite.2021.101229.

- [22] B. Mahanthesh, B. J. Giresha and R. S. R. Gorla, Nonlinear radiative heat transfer in MHD three-dimensional flow of water based nanofluid over a non-linearly stretching sheet with convective boundary condition, *Journal of the Nigerian Mathematical Society* **35**(1) (2016), 178 – 198, DOI: 10.1016/j.jnmms.2016.02.003.
- [23] S. Nandi, B. Kumbhakar, G. S. Seth and A. J. Chamkha, Features of 3D magneto-convective nonlinear radiative Williamson nanofluid flow with activation energy, multiple slips and Hall effect, *Physica Scripta* **96** (2021), 065206, DOI: 10.1088/1402-4896/abf009.
- [24] P. D. Prasad, R. V. M. S. S. K. Kumar and S. V. K. Varma, Heat and mass transfer analysis for the MHD flow of nanofluid with radiation absorption, *Ain Shams Engineering Journal* **9**(4) (2018), 801 – 813, DOI: 10.1016/j.asej.2016.04.016.
- [25] K. Raghunath, N. Gulle, R. R. Vaddemani and O. Mopuri, Unsteady MHD fluid flow past an inclined vertical porous plate in the presence of chemical reaction with aligned magnetic field, radiation, and Soret effects, *Heat Transfer* **51**(3) (2022), 2742 – 2760, DOI: 10.1002/htj.22423.
- [26] S. P. Samrat, C. Sulochana and G. P. Ashwinkumar, Impact of thermal radiation on an unsteady Casson nanofluid flow over a stretching surface, *International Journal of Applied and Computational Mathematics* **5** (2019), Article number: 31, DOI: 10.1007/s40819-019-0606-2.
- [27] G. S. Seth and M. K. Mishra, Analysis of transient flow of MHD nanofluid past a non-linear stretching sheet considering Navier’s slip boundary condition, *Advanced Powder Technology* **28**(2) (2017), 375 – 384, DOI: 10.1016/j.appt.2016.10.008.
- [28] S. Shateyi, Thermal radiation and buoyancy effects on heat and mass transfer over a semi-infinite stretching surface with suction and blowing, *Journal of Applied Mathematics* **2008** (2008), Article ID 414830, 12 pages, DOI: 10.1155/2008/414830.
- [29] S. Shateyi and S. S. Motsa, Thermal radiation effects on heat and mass transfer over an unsteady stretching surface, *Mathematical Problems in Engineering* **2009** (2009), Article ID 965603, pages 13, DOI: 10.1155/2009/965603.
- [30] A. K. Singha, G. S. Seth, K. Bhattacharyya, D. Yadav, A. K. Verma and A. K. Gautam, Soret and Dufour effects on hydromagnetic flow of H₂O-based nanofluids induced by an exponentially expanding sheet saturated in a non-Darcian porous medium, *Journal of Nanofluids* **10**(4) (2021), 506 – 517, DOI: 10.1166/jon.2021.1800.
- [31] S. Sivasankaran, M. A. Mansour, A. M. Rashad and M. Bhuvanewari, MHD mixed convection of Cu–water nanofluid in a two-sided lid-driven porous cavity with a partial slip, *Numerical Heat Transfer, Part A: Applications – An International Journal of Computation and Methodology* **70**(12) (2016), 1356 – 1370, DOI: 10.1080/10407782.2016.1243957.
- [32] C. Sulochana, G. P. Ashwinkumar and N. Sandeep, Effect of frictional heating on mixed convection flow of chemically reacting radiative Casson nanofluid over an inclined porous plate, *Alexandria Engineering Journal* **57**(4) (2018), 2573 – 2584, DOI: 10.1016/j.aej.2017.08.006.
- [33] R. R. Vaddemani, R. Kodi and O. Mopuri, Characteristics of MHD Casson fluid past an inclined vertical porous plate, *Materials Today: Proceedings* **49**(5) (2022), 2136 – 2142, DOI: 10.1016/j.matpr.2021.08.328.

